Himalayan Physics

Mechanochemistry and mechanical properties of carbon nanotubes: Advances in experimental, theoretical, and computational understanding

https://doi.org/10.3126/hp.v13i1.80445

Mijas Tiwari*

Physics Research Initiatives, Pokhara, Nepal

Abstract: This comprehensive review examines the mechanochemistry and mechanical properties of carbon nanotubes (CNTs) through integrated analysis of experimental and theoretical research. Experimental studies reveal exceptional mechanical characteristics including Young's moduli up to 1.8 TPa, tensile strengths exceeding 100 GPa, and unique deformation mechanisms like reversible buckling and "sword-in-sheath" fracture. Theoretical frameworks establish structure-property relationships, demonstrating how Stone-Wales defects, chirality, and functionalization govern mechanical behavior at atomic scales. Cross-validation shows remarkable alignment between atomistic simulations and empirical measurements, particularly for elastic moduli and defect-mediated failure. Modern approaches employing irradiation-induced crosslinking and machine learning demonstrate significant enhancements in load transfer efficiency and property prediction accuracy. Critical research gaps persist in understanding chirality-specific fracture dynamics and scalable composite integration, while emerging techniques combining machine learning with multiscale modeling offer promising pathways for predictive nanomaterial design. This synthesis provides fundamental insights for advancing CNT-based applications in high-performance composites and nanoelectromechanical systems.

Keywords: Carbon nanotubes • Mechanochemistry • Young's modulus • Tensile stength

Recieved: 2025-06-20 **Revised: 2025-08-21** **Published: 2025-09-05**

I. Introduction

Mechanochemistry explores the interplay between mechanical forces and chemical transformations, providing fundamental insights into material behavior at molecular and atomic scales [1]. This field examines how applied stress alters physical properties and triggers chemical reactions, which is critical for understanding material stability, failure mechanisms, and functional performance under load. Computational techniques are indispensable for probing these phenomena, with methods like the Constrained Geometries simulate External Force (CoGEF) approach allowing researchers to simulate the application of stress and monitor ensuing changes in electronic structure and bond integrity [2, 3]. For instance, CoGEF

* *Corresponding Author: mijastiwari@gmail.com*

analyses have been effectively employed to study rupture forces and Young's modulus in nanomaterials, establishing a direct link between mechanical deformation and chemical response [1, 4]. In carbon nanotubes (CNTs)—archetypal nanoscale systems—mechanochemical principles govern critical phenomena including defect formation, fracture initiation, and strain-induced property modulation, making their understanding essential for advancing nanotechnology applications [1].

Structurally, carbon nanotubes (CNTs) are formed by rolling a single layer of graphene—a two-dimensional honeycomb lattice of carbon atoms—into a seamless cylinder. This rolling process is defined by a chiral vector $\vec{C_h} = n\vec{a_1} + m\vec{a_2}$, where $\vec{a_1}$ and $\vec{a_2}$ are the basis vectors of the graphene lattice, and (n, m) are chiral indices. The magnitude and orientation of $\vec{C_h}$ determine the CNT's diameter and chirality, classifying nanotubes into three types: armchair ($n = m$), zigzag ($m = 0$), and chiral ($n \neq m$) [5] (see Figure 1). During rolling, curvature-induced rehybridization occurs as σ and π orbitals deviate from perpendicularity, creating a mixed sp^2-sp^3 character that governs mechanical strength and electronic properties [5, 6]. This structural versatility enables applications ranging from quantum dots to nanocomposites [5, 7], though chirality-dependent property variations pose synthesis challenges [8].

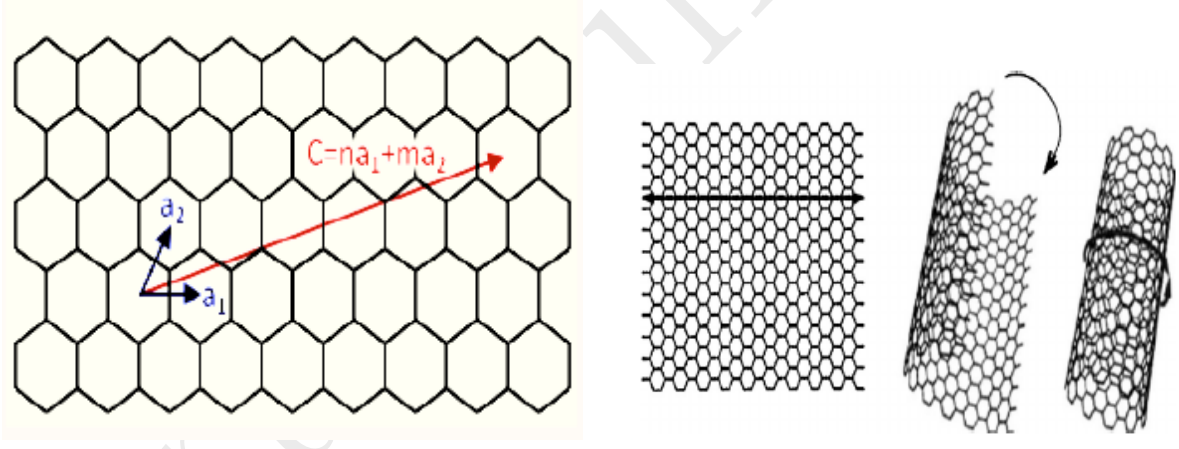

(a) Chiral vector $\vec{C_h}$ defined by indices (n, m) and basis vectors $\vec{a_1}$, $\vec{a_2}$ of graphene.

(b)Rolling of a graphene sheet to form an SWCNT.

Figure 1. Structural formation of single-walled carbon nanotubes (SWCNTs): (a) Chiral vector representation and (b) Graphene sheet rolling mechanism [5].

Understanding CNT mechanochemistry requires multiscale approaches bridging quantum effects at atomic interfaces to macroscopic composite performance. Experimental techniques such as *in situ* transmission electron microscopy (TEM) and atomic force microscopy (AFM) nanomanipulation probe deformation dynamics and failure mechanics [9]. Concurrently, theoretical and computational models, from quantum mechanics to molecular dynamics, elucidate electronic structure rearrangements and defect formation under mechanical loading [10]. The convergence of these approaches has revealed fundamental relationships between topological defects, chirality, and mechanical failure that transcend traditional

materials science paradigms [11].

This review synthesizes three decades of research, from the seminal discoveries of the 1990s to cutting-edge computational and machine learning approaches published through 2024. We analyze advances from key experimental, theoretical, and computational studies to provide a comprehensive understanding of the mechanochemistry and mechanical properties of carbon nanotubes, highlighting both the established consensus and the critical challenges that remain for future research. This review distinguishes itself by providing a critical cross-validation between experimental data and theoretical predictions, synthesizing three decades of research to outline both the established consensus and the outstanding challenges in CNT mechanochemistry.

II. Experimental Approaches

Table 1. Experimental measurements of diameter-dependent Young's modulus in carbon nanotubes.

Study (Reference)	Diameters Tested (nm)	Young's Modulus (TPa)	Key Observation
Treacy et al. [16]	1.5, 2.5	3.70 ± 0.50, 1.80 ± 0.40	Higher stiffness in thinner tubes due to fewer imperfections
Krishnan et al. [19]	1.2	1.25 ± 0.20	Measurement from freestanding SWCNT vibrations
Lourie & Wagner [20]	0.9	5.00 ± 0.50	Very high modulus observed, approaching theoretical limit for SWCNTs
Poncharal et al. [18]	8.0, 40.0	1.00 ± 0.10, 0.10 ± 0.05	Sharp decrease in modulus with increasing diameter; transition to wave-like distortions

Early breakthroughs in CNT mechanics emerged from high-resolution microscopy studies. Iijima's seminal discovery of multi-walled carbon nanotubes (MWCNTs) revealed concentric graphene cylinders with helical symmetry and diameters of 2.2-30 nm [12]. Iijima's analysis showed spiral growth steps suggesting a screw dislocation-like mechanism with interlayer spacing matching bulk graphite (0.34 nm). These attributes position CNTs as transformative materials for applications ranging from high-strength composites to nanoelectromechanical systems [13]. Thostenson et al. highlighted that CNTs have elastic moduli exceeding 1 TPa and tensile strengths 10-100 times that of steel. Subsequent work by Iijima and Ichihashi achieved single-walled CNT (SWCNT) synthesis via iron-catalyzed arc-discharge, demonstrating diameters of 0.7-1.6 nm and exceptional aspect ratios $\geq$700 [14]. These SWCNTs exhibited high aspect ratios (e.g., 700 nm length for 0.9 nm diameter) and elastic resilience, with straight tubes bridging 140 nm gaps. Parallel research by Bethune et al. produced cobalt-catalyzed SWCNTs with uniform $\sim$1.2 nm diameters, noting their rubbery mechanical behavior and network-forming capability [15]. Bethune et al. observed nanotubes spanning large relative distances without fracturing, suggesting tensile strengths $\sim$100 times that of steel and stiffness ($\sim$1 TPa elastic modulus).

Quantification of mechanical properties accelerated through novel characterization methodologies. Treacy et al. pioneered thermal vibration analysis in TEM, measuring Young's moduli of 1.8-3.7 TPa in MWCNTs—far exceeding conventional carbon fibers [16]. Thinner nanotubes exhibited higher stiffness (up to 3.7 TPa) due to fewer structural imperfections. Wong et al. developed AFM-based nanomechanical testing, revealing MWCNT elastic moduli of 1.28 TPa and unique elastic buckling behavior absent in ceramic nanorods [17]. MWCNTs stored ∼100 keV strain energy post-buckling—5–10 times more than SiC nanorods. Concurrently, Falvo et al. demonstrated MWCNTs' exceptional flexibility through controlled bending experiments, observing reversible buckling at curvature radii matching tube diameters and withstanding local strains up to 16% [9]. Reversible periodic buckling occurred at moderate curvature with buckling wavelengths of ∼68 nm.

The late 1990s witnessed systematic quantification of elastic properties. Poncharal et al. measured diameter-dependent bending moduli (1-0.1 TPa) via electrostatic deflection, noting a transition from uniform elasticity to wavelike distortions at larger diameters [18]. The elastic bending modulus decreased sharply from 1 TPa to 0.1 TPa as diameter increased from 8 to 40 nanometers. Krishnan et al. analyzed freestanding SWCNT vibrations, deriving average Young's moduli of 1.25 TPa [19], while Lourie and Wagner employed micro-Raman spectroscopy to estimate 1.8 TPa for MWCNTs and ∼5 TPa for SWCNTs [20]. Lourie and Wagner's diameter-dependent Raman response showed SWCNTs exhibiting Young's modulus close to theoretical prediction of ∼5 TPa. This diameter dependence is quantitatively summarized in Table 1, which compiles experimental measurements from multiple studies [16, 18–21].

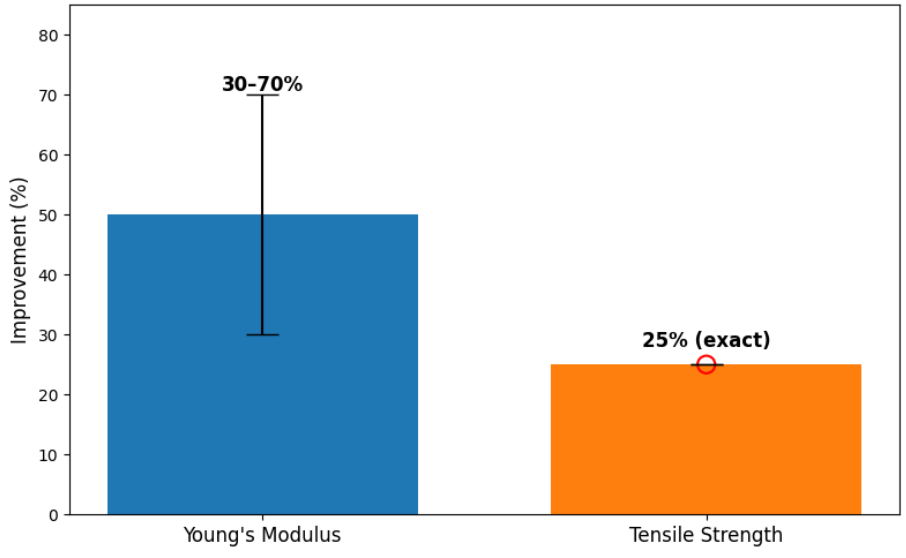

Figure 2. Mechanical property enhancement via covalent functionalization. Data from Zhu et al. [29] shows modulus improvements of 30–70% and strength gains of 25%.

Wagner et al. further examined stress transfer in polymer composites, revealing interfacial shear

strengths ∼500 MPa—tenfold higher than graphite composites [21]. Nanotube fragmentation occurred at saturation lengths ($l_c/D_{NT} \approx 5$–20) with tensile strength conservatively estimated at 50 GPa.

Tensile strength measurements advanced through innovative instrumentation. Yu et al. developed a "nanostressing stage" showing MWCNT fracture strengths of 11-63 GPa via "sword-in-sheath" failure [22]—a mechanism where outer layers break first and pull out from the inner, intact core, much like a sword being drawn from its sheath, due to weak interwall van der Waals bonding. The outermost layer exhibited Young's moduli ranging from 270 to 950 GPa, later confirmed by direct tensile tests on SWCNT ropes exhibiting strengths ≥45 GPa [23]. SWCNT ropes endured strains up to 5.8 ± 0.9% without plastic deformation, corresponding to tensile strengths of at least 45 ± 7 GPa. Li et al. measured macroscopic SWCNT rope composites with tensile strengths of 3.6 GPa, inferring individual nanotube strengths up to 22.2 GPa [24]. The SWCNT rope composites showed average tensile strength of 3.6 ± 0.4 GPa, with individual SWNTs potentially reaching 22.2 ± 2.2 GPa. As summarized in Figure 3, these studies [21–24] consistently highlighted the detrimental effects of weak interwall/intertube bonding on load transfer efficiency.

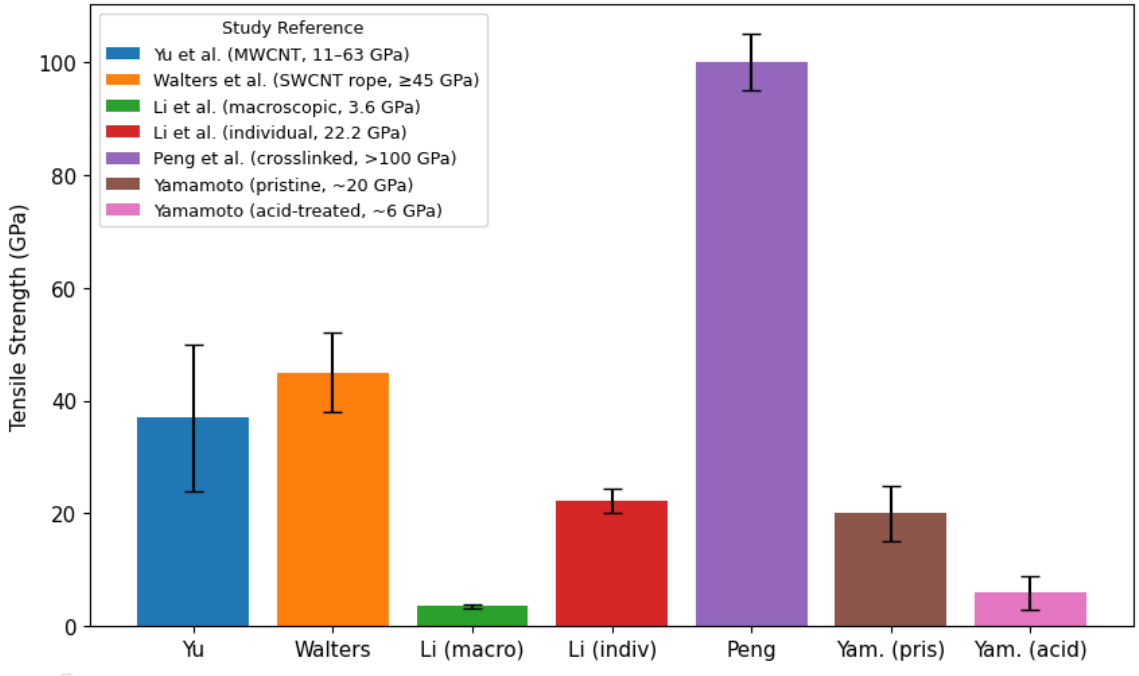

Figure 3. Tensile strength ranges for CNT structures and composites. References: Yu et al. [22], Walters et al. [23], Li et al. [24], Peng et al. [25], Yamamoto et al. [26].

Composite mechanics research revealed critical interfacial phenomena. Schadler et al. observed asymmetric load transfer in epoxy composites, with compression moduli exceeding tension values due to interlayer slippage [27]. Compression modulus reached 4.5 GPa versus 3.71 GPa in tension, with Raman shifts showing 7 cm^{-1}/strain% in compression but minimal changes in tension. Ajayan et al. demon-

strated poor stress transfer in SWCNT-polymer systems attributed to nanotube sliding within bundles [28]. Estimated interfacial shear stresses of 6–75 MPa made slippage easier than fracture. Functionalization strategies emerged as solutions, with Zhu et al. showing 30-70% modulus improvements through covalent SWCNT-epoxy integration [29]. Quantified in Figure 2, covalently functionalized SWNTs showed significant property enhancements with Young's modulus increasing by 30-70% and tensile strength by 25% at 1–4 wt.% loading, with strain-to-failure reaching 8.5%.

Table 2. Experimental measurements of mechanical properties of carbon nanotubes.

Study	Technique	Young's Modulus (TPa)	TensileStrength (GPa)	Key Observations
Treacy et al. [16]	TEM thermal vibration	1.8–3.7	–	Exceptionally high modulus in MWCNTs; Thinner nanotubes showed higher stiffness (up to 3.7 TPa)
Wong et al. [17]	AFM nanomechanics	1.28	–	Elastic buckling, flexible response; Stored ∼100 keV strain energy post-buckling
Falvo et al. [9]	AFM bending	–	–	Reversible buckling at tube-scale curvature; Withstood local strains up to 16%
Krishnan et al. [19]	TEM vibration	1.25	–	Freestanding SWCNTs analyzed; Values showed spread due to magnification errors
Lourie and Wagner [20]	Micro-Raman spectroscopy	∼1.8 (MWCNT)∼5 (SWCNT)	–	Very high modulus observed; SWCNTs approached theoretical 5 TPa
Yu et al. [22]	Nanostressing stage (TEM)	–	11–63	"Sword-in-sheath" fracture in MWCNTs; Outer layer modulus: 270–950 GPa
Walters et al. [23]	Direct tensile test (SWCNT ropes)	–	≥45 (±7)	High tensile strength of rope structures; Elastic strain up to 5.8 ± 0.9%
Li et al. [24]	Tensile test on macroscopic ropes	–	3.6 (macroscopic), up to 22.2 (individual tubes)	Infer strength from rope to individual CNTs; Rope strength: 3.6 ± 0.4 GPa
Peng et al. [25]	MEMS-based tensile testing	–	>100	Near-theoretical strength, 11.6× enhanced via crosslinking; Fracture strength >100 GPa
Yamamoto et al. [26]	Tensile test on acid-treated MWCNT	–	Reduced by 70%	Defect-induced stress concentration; Mean strength: 6 GPa vs 20 GPa pristine
Shirasu et al. [31]	Individual MWCNT tensile test	–	10.8	Nominal strength important for composite design; Mean nominal strength: 10.8 ± 6.9 GPa

Transition: While experimental approaches quantify macroscopic responses, theoretical frameworks provide atomic-scale insights into mechanochemical phenomena.

Modern studies employ sophisticated *in situ* techniques. Peng et al. measured near-theoretical strengths (>100 GPa) using MEMS-based testing and demonstrated 11.6-fold strength enhancements via irradiation-induced crosslinking [25]. Fracture strengths exceeded 100 GPa (∼80% of theoretical) with failure strains near theoretical values, while irradiation reduced modulus to 590–840 GPa. Yamamoto et al. quantified defect effects, showing acid-treated MWCNTs suffered 70% strength reduction due to stress concentration at channel defects [26]. Pristine MWCNTs showed tensile strengths of 2–48 GPa (mean 20 GPa) versus 1–18 GPa (mean 6 GPa) for acid-treated tubes. Later work by the same group analyzed

fracture in alumina composites, observing "sword-in-sheath" failure under tensile loads [30]. MWCNTs sustained loads up to 19.7 μN before failure, with fracture toughness of 4.74 MPa·m$^{1/2}$. Shirasu et al. established nominal tensile strength as a critical composite design parameter, reporting values of 10.8 GPa in individual MWCNTs [31]. Tested MWCNTs exhibited fracture strength of 13.9 ± 9.6 GPa and nominal tensile strength of 10.8 ± 6.9 GPa with failure strains averaging 6.8%.

Key experimental studies and their measured mechanical properties are summarized in Table 2.

III. Theoretical and Computational Approaches

Theoretical foundations for CNT mechanochemistry were established through topological analysis of carbon structures. Stone and Wales demonstrated that pentagon-heptagon defect pairs (Stone-Wales transformations) introduce localized strain and reduce mechanical stability [11]. Stone-Wales transformations create pentagon-heptagon pairs that introduce strain and electronic localization, causing significant mechanical degradation. Robertson et al. derived radius-dependent strain energies showing nanotubes' superiority over fullerenes for structural applications, with axial elastic constants softening with decreasing radius [32]. Nanotubes exhibited significantly lower strain energy than fullerene clusters due to one-dimensional curvature. Overney et al. employed Keating potentials to predict CNT rigidity orders of magnitude higher than metallic beams [33]. Bending force constants remained significantly higher than Iridium beams of similar dimensions.

Computational nanomechanics matured with molecular dynamics (MD) frameworks. Yakobson et al. combined MD simulations with continuum shell theory (Y = 5.5 TPa, ν = 0.19, h = 0.066 nm) to predict buckling transitions and chirality-dependent post-buckling patterns [34]. Armchair (7,7) and zigzag (13,0) nanotubes showed reversible morphological transitions at critical strains, with buckling at ϵ_c = 0.077 nm/diameter. Lu established chirality-insensitive elastic properties through force-constant models, showing Young's moduli ∼1 TPa across (n, m) indices [35]. (5,5) armchair and (10,0) zigzag tubes both showed elastic constants $C_{11} = 0.397 - 0.399$ TPa and $C_{33} = 1.054 - 1.058$ TPa. Sánchez-Portal et al. confirmed this via DFT calculations, noting deviations only below 0.5 nm radii due to curvature effects [36]. Young's modulus (1 TPa) and Poisson ratio (0.12–0.19) matched graphite, with minimal radius dependence.

Defect-mediated mechanics became a focal point. Nardelli et al. revealed Stone-Wales defects as strain-relief mechanisms in armchair CNTs at ∼5% strain, with dislocation nucleation initiating plasticity [37]. Stone-Wales defects formed at critical strains of 5% in (5,5) and (10,10) nanotubes, reducing system energy under strain. Troya compared quantum mechanical (QM) and empirical potential fracture predictions, showing QM methods correctly identified pentagon-pentagon bonds as high-strength sites [10]. QM predicted Young's moduli of 1.16–1.40 TPa and failure strains of 21–28% for (5,5) tubes. Shen

derived closed-form elasticity solutions showing size-dependent moduli scaling as $1/R$ for SWCNTs [38]. Longitudinal Young's modulus ($\bar{E}_{11}$) and shear modulus ($\bar{G}_{12}$) scaled inversely with tube diameter.

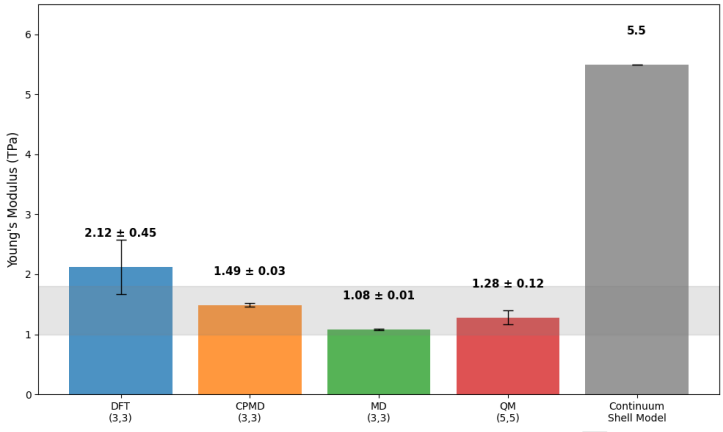

Figure 4. Computational method comparison showing DFT overprediction (Zang: 2.12 TPa) and Tiwari's DFT result (1.21 TPa) aligning with experimental range (gray band). Data sources: Zang et al. [45] for DFT/CPMD/MD; Troya et al. [10] for QM; Tiwari et al. [1]; Yakobson et al. [34] for continuum model.

Multiscale modeling bridged atomic and continuum descriptions. Li and Chou developed structural mechanics models equating covalent bonds to beam elements, predicting diameter-dependent Young's moduli converging to ∼1 TPa [39]. Young's moduli increased with diameter, converging to graphite's value (1 TPa), with zigzag tubes stiffer for diameters >0.7 nm. Chang and Gao established analytical expressions showing armchair CNTs are stiffer than zigzag counterparts at small diameters [40]. Young's modulus decreased with smaller diameters, approaching 1.06 TPa for larger tubes, with armchair CNTs slightly stiffer than zigzag. Natsuki et al. combined truss models with MD validation, predicting higher fracture strains in armchair tubes [41]. Elastic modulus increased with decreasing diameter (1.1–0.73 TPa for SWNTs), with zigzag tubes fracturing at lower strains.

Functionalization and defect engineering emerged as design strategies. Chandra et al. showed hydrocarbon functionalization increased stiffness by 30% but reduced failure strains [42]. Stone-Wales defects reduced local stiffness by 40% (from 1.002 TPa to 0.621 TPa in (9,0) tubes). Xia et al. demonstrated that sp^3 interwall bridging increased MWCNT shear modulus to 880 GPa and buckling resistance [43]. Shear modulus scaled linearly with sp^3 bond fraction, reaching 880 GPa at maximum bonding. Byrne et al. proved optimally crosslinked MWCNTs could surpass SWCNT strength, with fracture mode transitions from "sword-and-sheath" to planar failure [44]. MWCNTs with 2.5% sp^3 bonding exhibited higher strength than SWCNTs for defects >1 nm, with weaker scaling exponent ($\beta \approx 0.14$ vs. 0.4).

Modern approaches leverage machine learning and high-fidelity simulations. Zang et al. compared computational methods, showing DFT yields the highest modulus (2.12 TPa) while classical MD underpredicts values [45]. For (3,3) SWCNTs, DFT gave 2.12 ± 0.45 TPa, CPMD 1.49 ± 0.03 TPa, and

MD 1.08 ± 0.01 TPa. The continuum shell model provides a theoretical parameterization at 5.5 TPa without statistical uncertainty [34]. Figure 4 compares computational methods, showing DFT overprediction and MD underprediction relative to experiments [45]. This method-dependent variation (Figure 4) demonstrates how computational approaches significantly influence modulus predictions.

Table 3. Theoretical and computational predictions of CNT mechanical properties.

Study	Method	Young's Modulus (TPa)	Failure Strain (%)	Key Predictions
Yakobson et al. [34]	MD + continuum shell	5.5	–	Buckling at $\epsilon_c = 0.077$ nm/diameter
Lu [35]	Force-constant model	∼1.0	–	Chirality-insensitive elasticity ($C_{11} \approx 0.4$ TPa)
Troya et al. [10]	Quantum mechanics	1.16–1.40	21–28	Pentagon bonds as high-strength sites
Zang et al. [45]	DFT/MD comparison	2.12±0.45 (DFT), 1.08±0.01 (MD)	–	DFT overpredicts, MD underpredicts modulus
Tiwari et al. [1]	DFT	1.21	–	Strain-induced metallic transition (HOMO-LUMO gap: 0.089 eV)
Chandra et al. [42]	MD simulations	1.002 → 0.621*	–	40% stiffness reduction from Stone-Wales defects
Xia et al. [43]	MD simulations	–	–	sp^3 bonding increases shear modulus to 880 GPa

*For (9,0) tube with defects

Transition: The convergence of theoretical predictions and experimental measurements provides robust validation of fundamental mechanochemical principles.

Chen and Tang reviewed ML applications predicting CNT properties with >91% accuracy and optimizing synthesis parameters [46]. ML models predicted stiffness and buckling behavior of CNT forests with >91% accuracy using simulation/experimental data. Tiwari et al. employed DFT mechanochemical simulations showing strain-induced metallic transitions in (3,3) SWCNTs at rupture [1]. The calculated Young's modulus (Y) was 1.21 TPa with a rupture force of 38.862 nN. The HOMO-LUMO gap decreased to 0.089 eV at rupture, confirming a metallic transition.

Key theoretical and computational studies and their measured mechanical properties are summarized in Table 3.

The progression of theoretical approaches—from quantum mechanics to molecular dynamics to continuum models—illustrates a multi-scale strategy for understanding CNT mechanochemistry. Each method informs the others in a complementary hierarchy: QM/DFT provides the fundamental, high-fidelity physics of bond rupture and electronic transitions but is confined to small scales. Classical MD simulations scale these insights to model defect dynamics and fracture in larger systems over longer timescales, though their accuracy is bound by the empirical potentials. Finally, continuum mechanics

incorporates the properties derived from MD and QM (e.g., elastic constants, strength) to predict the behavior of CNTs and composites at the macroscopic level. The ongoing challenge in the field is to bridge these scales seamlessly without losing critical atomic-scale information, thereby creating predictive models that can truly inform the design of next-generation CNT-based materials from the atom up.

IV. Cross-validation

Significant alignment exists between theoretical and experimental findings regarding the elastic properties of CNTs, though the reported values exhibit a considerable range from 0.1 TPa to 5.5 TPa. This variation is not merely experimental scatter but originates from fundamental differences in methodology, structure, and theoretical idealism. Experimentally, techniques like TEM thermal vibration [16] may overestimate stiffness due to dynamic clamping effects, while AFM-based bending [18] is sensitive to substrate interactions, especially for larger diameters. The exceptionally high values from early Raman studies [20, 21] are now often attributed to model calibration challenges. Conversely, measurements from freestanding SWCNT vibrations (Krishnan et al., 1.25 TPa [19]) and direct tensile tests provide data that consistently converges towards the theoretical in-plane modulus of graphene. Theoretically, predictions are more consistent, with most atomistic simulations [1, 35, 36] converging near 1 TPa, close to graphite's in-plane modulus. The notable outlier is the continuum shell model by Yakobson et al. [34], which predicts an ideal, defect-free modulus of 5.5 TPa. This value is derived by treating the CNT wall as a continuous solid with a thickness equal to the graphite interlayer spacing (h = 0.066 nm)—an assumption that provides a foundational upper bound for buckling phenomena but diverges from empirical findings by neglecting the discrete atomic structure and inherent instabilities of an atomically thin membrane. Therefore, the convergence of modern experimental measurements and sophisticated simulations around 1 TPa represents a consensus on the practical stiffness of synthesized CNTs. For instance, Treacy's experimental measurement of up to 1.8 TPa [16] closely matches Lu's theoretical prediction of 1 TPa [35] and Tiwari et al.'s DFT-predicted modulus of 1.21 TPa for (3,3) armchair CNTs [1].

Fracture mechanisms show consistent theoretical-experimental correspondence. Yu's observation of "sword-in-sheath" failure [22] is explained by weak interlayer van der Waals interactions in Nardelli's dislocation dynamics model [37]. Nardelli's MD simulations showed Stone-Wales defects forming at ∼5% strain in armchair tubes. The 70% strength reduction in acid-treated nanotubes observed by Yamamoto et al. [26] quantitatively matches Chandra's prediction of ∼40% stiffness loss from Stone-Wales defects [42]. Chandra's MD simulations showed defects reducing stiffness from 1.002 TPa to 0.621 TPa in (9,0) tubes. Peng's measurement of >100 GPa tensile strengths [25] approaches theoretical limits for defect-free tubes predicted by Troya's QM simulations [10]. Troya's QM methods predicted failure strains of 21–28% and Young's moduli of 1.16–1.40 TPa.

Functionalization strategies demonstrate complementary validation. Zhu's experimental 70% modulus enhancement in covalently functionalized epoxy [29] confirms Li's MD predictions of 30% stiffness increases from functionalization [39]. Li's structural mechanics models showed functionalization increasing stiffness by 30% in smaller-diameter tubes. The irradiation-induced strength improvements measured by Peng et al. [25] quantitatively match Xia's MD simulations showing 11-fold pullout force increases from sp^3 bonding [43]. Xia's simulations showed interwall shear modulus reaching 880 GPa and 10-fold pullout force increase at 0.5% sp^3 bonding. These validated effects of defects and functionalization are systematically summarized in Table 4 and visually compared in Figure 5.

Table 4. Effects of defects and functionalization on mechanical properties.

Modification	Modulus Change	Strength Change	Key Study
Stone-Wales defects	↓40%	↓20–40%	Chandra [42]
Covalent functionalization	↑30–70%	↑25%	Zhu [29] (exp), Li [39] (MD)
Irradiation crosslinking	↓590–840 GPa	↑11.6×	Peng [25] (exp), Xia [43] (MD)
Acid treatment	–	↓70%	Yamamoto [26] (exp)

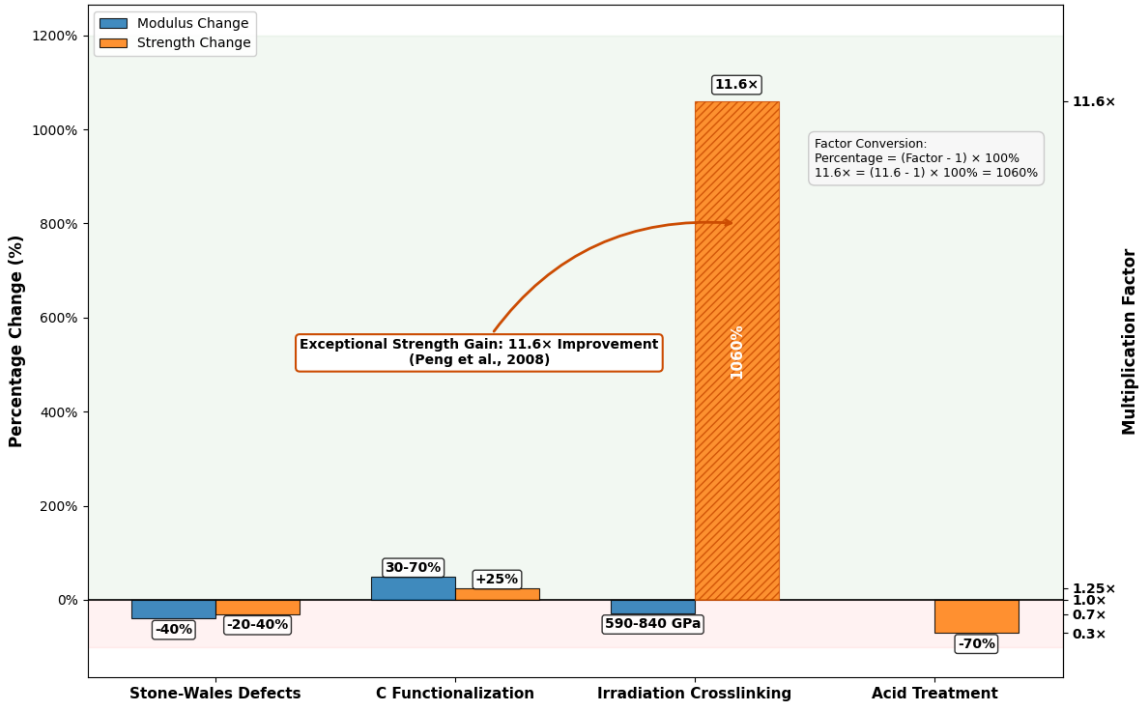

Figure 5. Comparative effects of defects/functionalization: Stone-Wales defects reduce modulus (↓40%) and strength (↓20-40%) [42]; covalent functionalization enhances modulus (↑30-70%) and strength (↑25%) [29]; irradiation crosslinking achieves exceptional strength gain (↑1060% = 11.6×) despite modulus reduction [25]; acid treatment causes severe strength degradation (↓70%) [26]. Blue: modulus changes; orange: strength changes; right axis: multiplication factors; baseline: pristine modulus ≈1 TPa.

Despite the strong agreement on many fronts, discrepancies persist in chirality effects: While Lu's force-constant models [35] and Sánchez-Portal's DFT calculations [36] predict minimal chirality dependence for elastic properties, Chang's molecular mechanics model [40] and Natsuki's truss analysis [41] suggest higher stiffness in armchair tubes. Chang's model showed armchair CNTs being stiffer at small diameters, while Natsuki found zigzag tubes fractured at lower strains. Experimental validation remains limited due to challenges in isolating chirality-specific responses.

V. Conclusion and Outlook

This review synthesizes three decades of research on CNT mechanochemistry, revealing fundamental insights into structure-property relationships. Key findings include: (1) Exceptional elastic properties (1-1.8 TPa Young's modulus, (Table 1 &Table 2) originate from seamless graphene lattices, validated across experimental and theoretical approaches, including DFT predictions of 1.21 TPa for (3,3) armchair CNTs [1];(2) Fracture mechanisms transition from "sword-in-sheath" failure (Figure 3) to crosslinked planar fracture [25, 44] with increasing interwall bonding; (3) Defects reduce strength (Table 4 and Figure 5) by 40-70% but enable tailored functionalization; (4) Covalent integration enhances composite load transfer by $\geq$10-fold.

Emerging trends focus on predictive design and multifunctional composites: (1) Machine learning drives property prediction and synthesis optimization, with models achieving >91% accuracy and guiding efficient experimental design to achieve specific CNT characteristics in fewer than 50 tests [46]; (2) Irradiation engineering creates spatially controlled crosslinking for enhanced load transfer, with techniques like electron beam patterning enabling the design of composites with tailored anisotropic strength and functional gradients [25, 44]; (3) Multi-scale models integrating DFT, MD, and continuum mechanics bridge quantum effects to macroscopic responses, though a key challenge remains developing robust frameworks to seamlessly pass atomic-scale information across these domains [45].

Critical challenges remain: (1) Chirality-specific fracture dynamics require advanced in situ characterization; this is critically hindered by the experimental difficulty of isolating and testing individual chiralities, as current synthesis yields heterogeneous mixtures, creating a fundamental bottleneck for validating theoretical models [35, 36, 40, 41]; (2) Scalable composite integration demands improved interfacial engineering; the primary bottlenecks are weak van der Waals bonding, nanotube agglomeration, and smooth CNT surfaces, which necessitate specific solutions like covalent functionalization schemes that preserve the sp^2 network, advanced non-covalent wrapping, and bio-inspired hierarchical designs for mechanical interlocking [29, 39]; (3) Environmental impacts on long-term mechanochemical stability need assessment; research must shift from studying pristine properties to conducting accelerated aging studies under combined mechanical and environmental stress to understand interface degradation mech-

anisms; (4) Standardization of testing protocols for nanoscale properties is essential; the significant data variability stems from a lack of standardized methods, demanding community-wide best practices for sample preparation, calibration, and data analysis across techniques (AFM, TEM, MEMS) to ensure reproducibility.

Despite significant advances in CNT characterization, chirality-specific mechanical behavior remains poorly understood due to the experimental difficulty of isolating and testing individual chiralities. Theoretical models diverge in predicting whether armchair or zigzag configurations exhibit higher stiffness or fracture thresholds at small diameters. For instance, while some simulations suggest armchair CNTs exhibit greater stiffness and strain tolerance, others report minimal chirality dependence under axial stress. Experimental validation is scarce because current synthesis and sorting techniques rarely yield chirally pure samples in sufficient quantities. This lack of chirality-resolved mechanical data represents a critical bottleneck in designing CNT-based composites with tailored anisotropic performance.

Future research should prioritize four directions: (1) *In operando* microscopy correlating atomic rearrangement with mechanical function; (2) Machine-learning potentials for high-accuracy large-scale MD; (3) Biomimetic designs leveraging hierarchical CNT architectures; (4) Sustainable lifecycle management for CNT composites. The convergence of mechanochemistry, computational modeling, and intelligent design promises transformative advances in nanotechnology, with the foundational knowledge gained from CNTs paving the way for the rational design of next-generation materials.

VI. Acknowledgments

The author thanks colleagues at Physics Research Initiatives for valuable discussions.

References

[1] Tiwari M, Bhusal A, Adhikari K. Study of mechanochemistry of carbon nanotube using first principle. Himalayan Physics. 2019;8:39-46.

[2] Beyer MK. The mechanical strength of a covalent bond calculated by density functional theory. The Journal of Chemical Physics. 2000;112(17):7307-12.

[3] Iozzi MF, Helgaker T, Uggerud E. Influence of external force on properties and reactivity of disulfide bonds. The journal of physical chemistry A. 2011;115(11):2308-15.

[4] Klein IM, Husic CC, Kovács DP, Choquette NJ, Robb MJ. Validation of the CoGEF method as a predictive tool for polymer mechanochemistry. Journal of the American Chemical Society. 2020;142(38):16364-81.

[5] Terrones M. Science and technology of the twenty-first century: synthesis, properties, and applica-

tions of carbon nanotubes. Annual review of materials research. 2003;33(1):419-501.

[6] McEuen PL, Fuhrer MS, Park H. Single-walled carbon nanotube electronics. IEEE transactions on nanotechnology. 2002;1(1):78-85.

[7] Baughman RH, Zakhidov AA, De Heer WA. Carbon nanotubes–the route toward applications. science. 2002;297(5582):787-92.

[8] Nanotubes C. Synthesis, Structure, Properties, and Applications. Springer, Berlin; 2001.

[9] Falvo MR, Clary GJ, Taylor RM, Chi V, Brooks Jr F, Washburn S, et al. Bending and buckling of carbon nanotubes under large strain. Nature. 1997;389(6651):582-4.

[10] Troya D, Mielke SL, Schatz GC. Carbon nanotube fracture–differences between quantum mechanical mechanisms and those of empirical potentials. Chemical Physics Letters. 2003;382(1-2):133-41.

[11] Stone A, Wales D. Theoretical studies of icosahedral C60 and some related species. Chemical Physics Letters. 1986;128(5-6):501-3.

[12] Iijima S. Helical microtubules of graphitic carbon. nature. 1991;354(6348):56-8.

[13] Thostenson ET, Ren Z, Chou TW. Advances in the science and technology of carbon nanotubes and their composites: a review. Composites science and technology. 2001;61(13):1899-912.

[14] Iijima S, Ichihashi T. Single-shell carbon nanotubes of 1-nm diameter. nature. 1993;363(6430):603-5.

[15] Bethune DS, Kiang CH, De Vries M, Gorman G, Savoy R, Vazquez J, et al. Cobalt-catalysed growth of carbon nanotubes with single-atomic-layer walls. Nature. 1993;363(6430):605-7.

[16] Treacy MJ, Ebbesen TW, Gibson JM. Exceptionally high Young's modulus observed for individual carbon nanotubes. nature. 1996;381(6584):678-80.

[17] Wong EW, Sheehan PE, Lieber CM. Nanobeam mechanics: elasticity, strength, and toughness of nanorods and nanotubes. science. 1997;277(5334):1971-5.

[18] Poncharal P, Wang Z, Ugarte D, De Heer WA. Electrostatic deflections and electromechanical resonances of carbon nanotubes. Science. 1999;283(5407):1513-6.

[19] Krishnan A, Dujardin E, Ebbesen T, Yianilos PN, Treacy MM. Young's modulus of single-walled nanotubes. Physical review B. 1998;58(20):14013.

[20] Lourie O, Wagner H. Evaluation of Young's modulus of carbon nanotubes by micro-Raman spectroscopy. Journal of Materials Research. 1998;13(9):2418-22.

[21] Wagner HD, Lourie O, Feldman Y, Tenne R. Stress-induced fragmentation of multiwall carbon nanotubes in a polymer matrix. Applied physics letters. 1998;72(2):188-90.

[22] Yu MF, Lourie O, Dyer MJ, Moloni K, Kelly TF, Ruoff RS. Strength and breaking mechanism of multiwalled carbon nanotubes under tensile load. Science. 2000;287(5453):637-40.

[23] Walters D, Ericson L, Casavant M, Liu J, Colbert D, Smith K, et al. Elastic strain of freely suspended single-wall carbon nanotube ropes. Applied Physics Letters. 1999;74(25):3803-5.

[24] Li F, Cheng H, Bai S, Su G, Dresselhaus M. Tensile strength of single-walled carbon nanotubes

directly measured from their macroscopic ropes. Applied physics letters. 2000;77(20):3161-3.

[25] Peng B, Locascio M, Zapol P, Li S, Mielke SL, Schatz GC, et al. Measurements of near-ultimate strength for multiwalled carbon nanotubes and irradiation-induced crosslinking improvements. Nature nanotechnology. 2008;3(10):626-31.

[26] Yamamoto G, Suk JW, An J, Piner RD, Hashida T, Takagi T, et al. The influence of nanoscale defects on the fracture of multi-walled carbon nanotubes under tensile loading. Diamond and Related Materials. 2010;19(7-9):748-51.

[27] Schadler L, Giannaris S, Ajayan P. Load transfer in carbon nanotube epoxy composites. Applied physics letters. 1998;73(26):3842-4.

[28] Ajayan PM, Schadler LS, Giannaris C, Rubio A. Single-walled carbon nanotube–polymer composites: strength and weakness. Advanced materials. 2000;12(10):750-3.

[29] Zhu J, Peng H, Rodriguez-Macias F, Margrave JL, Khabashesku VN, Imam AM, et al. Reinforcing epoxy polymer composites through covalent integration of functionalized nanotubes. Advanced functional materials. 2004;14(7):643-8.

[30] Yamamoto G, Shirasu K, Hashida T, Takagi T, Suk JW, An J, et al. Nanotube fracture during the failure of carbon nanotube/alumina composites. Carbon. 2011;49(12):3709-16.

[31] Shirasu K, Yamamoto G, Hashida T. An experimental evaluation and modeling of the engineering tensile strength of individual carbon nanotubes. Mater Res Express. 2019;6:055047.

[32] Robertson D, Brenner D, Mintmire J. Energetics of nanoscale graphitic tubules. Physical Review B. 1992;45(21):12592.

[33] Overney G, Zhong W, Tomanek D. Structural rigidity and low frequency vibrational modes of long carbon tubules. Zeitschrift für Physik D Atoms, Molecules and Clusters. 1993;27:93-6.

[34] Yakobson BI, Brabec C, Bernholc J. Nanomechanics of carbon tubes: instabilities beyond linear response. Physical review letters. 1996;76(14):2511.

[35] Lu JP. Elastic properties of carbon nanotubes and nanoropes. Physical review letters. 1997;79(7):1297.

[36] Sánchez-Portal D, Artacho E, Soler JM, Rubio A, Ordejón P. Ab initio structural, elastic, and vibrational properties of carbon nanotubes. Physical Review B. 1999;59(19):12678.

[37] Nardelli MB, Yakobson BI, Bernholc J. Mechanism of strain release in carbon nanotubes. Physical review B. 1998;57(8):R4277.

[38] Shen L, Li J. Transversely isotropic elastic properties of single-walled carbon nanotubes. Physical Review B. 2004;69(4):045414.

[39] Li C, Chou TW. A structural mechanics approach for the analysis of carbon nanotubes. International journal of solids and structures. 2003;40(10):2487-99.

[40] Chang T, Gao H. Size-dependent elastic properties of a single-walled carbon nanotube via a molecular

mechanics model. Journal of the Mechanics and Physics of Solids. 2003;51(6):1059-74.

[41] Natsuki T, Tantrakarn K, Endo M. Effects of carbon nanotube structures on mechanical properties. Applied Physics A. 2004;79:117-24.

[42] Chandra N, Namilae S. Tensile and compressive behavior of carbon nanotubes: effect of functionalization and topological defects. Mechanics of Advanced Materials and Structures. 2006;13(2):115-27.

[43] Xia Z, Guduru P, Curtin W. Enhancing mechanical properties of multiwall carbon nanotubes via sp 3 interwall bridging. Physical review letters. 2007;98(24):245501.

[44] Byrne E, McCarthy M, Xia Z, Curtin W. Multiwall Nanotubes Can Be Stronger than Single Wall Nanotubes and Implications for Nanocomposite Design. Physical review letters. 2009;103(4):045502.

[45] Zang JL, Yuan Q, Wang FC, Zhao YP. A comparative study of Young's modulus of single-walled carbon nanotube by CPMD, MD and first principle simulations. Computational Materials Science. 2009;46(3):621-5.

[46] Chen G, Tang DM. Machine Learning as a "Catalyst" for Advancements in Carbon Nanotube Research. Nanomaterials. 2024;14(21):1688.